

LA-UR 2- 96 - 0458

Los Alamos National Laboratory is operated by the University of California for the United States Department of Energy under contract W-7405-ENG-36

RECEIVED

APR 01 1996

TITLE: AN EXPONENTIAL DISCONTINUOUS SCHEME FOR X-Y
GEOMETRY TRANSPORT PROBLEMS

OSTI

AUTHOR(S): Todd A. Wareing
Raymond E. Alcouffee

SUBMITTED TO: Advancement in Applications in Radiation Protection Shielding
North Falmouth, Massachusetts
April 21-25, 1996

DISCLAIMER

This report was prepared as an account of work sponsored by an agency of the United States Government. Neither the United States Government nor any agency thereof, nor any of their employees, makes any warranty, express or implied, or assumes any legal liability or responsibility for the accuracy, completeness, or usefulness of any information, apparatus, product, or process disclosed, or represents that its use would not infringe privately owned rights. Reference herein to any specific commercial product, process, or service by trade name, trademark, manufacturer, or otherwise does not necessarily constitute or imply its endorsement, recommendation, or favoring by the United States Government or any agency thereof. The views and opinions of authors expressed herein do not necessarily state or reflect those of the United States Government or any agency thereof.

MASTER

By acceptance of this article, the publisher recognizes that the U.S. Government retains a nonexclusive royalty-free license to publish or reproduce the published form of this contribution or to allow others to do so, for U.S. Government purposes.

The Los Alamos National Laboratory requests that the publisher identify this article as work performed under the auspices of the U.S. Department of Energy.

DISTRIBUTION OF THIS DOCUMENT IS UNLIMITED 85

Los Alamos

Los Alamos National Laboratory
Los Alamos New Mexico 87545

AN EXPONENTIAL DISCONTINUOUS SCHEME FOR X-Y-Z GEOMETRY TRANSPORT PROBLEMS

Todd A. Wareing and Raymond E. Alcouffe
Los Alamos National Laboratory
P.O. Box 1663
Los Alamos, NM 87545
email: wareing@lanl.gov

ABSTRACT

The recently developed exponential discontinuous spatial differencing scheme for the discrete-ordinate equations has been extended to x-y-z geometry with hexahedral cells. This scheme produces strictly positive angular fluxes given positive discrete-ordinate sources. The exponential discontinuous scheme has been developed and implemented into the three-dimensional, discrete-ordinate code, THREEDANT. Numerical results are given which show that the exponential discontinuous scheme is very accurate for deep-penetration transport problems with optically thick spatial meshes.

I. INTRODUCTION

Recently, the algebraically equivalent nonlinear characteristic¹⁻³ (NC) and exponential characteristic⁴⁻⁵ (EC) spatial differencing schemes were developed. These schemes use the method of characteristics with an exponential representation for the discrete-ordinate source within each spatial cell. This source representation is derived using information theory⁶. The NC/EC scheme is very accurate, especially for deep-penetration problems with optically thick spatial cells. The NC/EC scheme also produces strictly positive angular fluxes given positive discrete-ordinate sources. Recently we developed an exponential discontinuous (ED) scheme in x-y geometry based upon an exponential representation for the angular flux within each cell⁷. This representation is also derived using information theory. The motivation for the ED scheme is that it is much less complicated to derive and implement than the NC/EC scheme and is assumed to be considerably less computationally expensive in x-y-z geometry. The NC/EC scheme is exact for pure-absorbing problems in all Cartesian geometries. The ED scheme is only exact for pure-absorbing problems in slab geometry. Nonetheless, the ED scheme appears to be nearly as accurate as the NC/EC scheme for many problems and also produces strictly positive angular fluxes. The ED scheme has been extended to x-y-z geometry with a hexahedral mesh and has been implemented into the three-dimensional, discrete-ordinate code, THREEDANTTM 8.

The remainder of the paper will proceed as follows: in Sec. II, we derive the ED scheme in x-y-z geometry and discuss the method of solution; in Sec. III, we present some numerical results to show the accuracy and positivity of the ED scheme; and in Sec IV, we conclude with a discussion.

II. THE EXPONENTIAL DISCONTINUOUS SCHEME

The mono-energetic, x-y-z geometry discrete-ordinate equations are given by

$$\begin{aligned} \mu_m \frac{\partial}{\partial x} \psi_m(x, y, z) + \eta_m \frac{\partial}{\partial y} \psi_m(x, y, z) + \xi_m \frac{\partial}{\partial z} \psi_m(x, y, z) \\ + \sigma_t(x, y, z) \psi_m(x, y, z) = S_m(x, y, z) \end{aligned} \quad (1)$$

Here $\psi_m(x, y, z)$ is the discrete ordinate angular flux and $S_m(x, y, z)$ is the discrete ordinate source comprised of a combination of scattering, fission or fixed sources. We use a hexahedral mesh with each spatial cell having dimensions $x_{i-1/2} \leq x \leq x_{i+1/2}$, $y_{j-1/2} \leq y \leq y_{j+1/2}$, and $z_{k-1/2} \leq z \leq z_{k+1/2}$. We assume that the material properties are constant within each mesh cell.

We begin our derivation of the ED scheme by taking the zeroth, x, y and z spatial coordinate moments of Eq.(1). This is done by multiplying Eq.(1) by 1, $P_1(x) = 2(x - x_i)/\Delta x_i$, $P_1(y) = 2(y - y_j)/\Delta y_j$ and $P_1(z) = 2(z - z_k)/\Delta z_k$, and integrating over the volume of the cell. Here $\Delta x_i = x_{i+1/2} - x_{i-1/2}$, $x_i = (x_{i-1/2} + x_{i+1/2})/2$, $\Delta y_j = y_{j+1/2} - y_{j-1/2}$, $y_j = (y_{j-1/2} + y_{j+1/2})/2$, $\Delta z_k = z_{k+1/2} - z_{k-1/2}$, and $z_k = (z_{k-1/2} + z_{k+1/2})/2$. This gives the following four moment balance equations:

$$\begin{aligned} \frac{\mu_m}{\Delta x_i} (\psi_{m,i-1/2,j,k} - \psi_{m,i+1/2,j,k}) + \frac{\eta_m}{\Delta y_j} (\psi_{m,i,j+1/2,k} - \psi_{m,i,j-1/2,k}) \\ + \frac{\xi_m}{\Delta z_k} (\psi_{m,i,j,k+1/2} - \psi_{m,i,j,k-1/2}) + \sigma_{t,i,j,k} \psi_{m,i,j,k} = S_{m,i,j,k} \end{aligned} \quad (2)$$

$$\begin{aligned} \frac{3\mu_m}{\Delta x_i} (\psi_{m,i+1/2,j,k} + \psi_{m,i-1/2,j,k} - 2\psi_{m,i,j,k}) + \frac{\eta_m}{\Delta y_j} (\psi_{m,i,j+1/2,k}^x - \psi_{m,i,j-1/2,k}^x) \\ + \frac{\xi_m}{\Delta z_k} (\psi_{m,i,j,k+1/2}^x - \psi_{m,i,j,k-1/2}^x) + \sigma_{t,i,j,k} \psi_{m,i,j,k}^x = S_{m,i,j,k}^x \end{aligned} \quad (3)$$

$$\begin{aligned} \frac{\mu_m}{\Delta x_i} (\psi_{m,i+1/2,j,k}^y - \psi_{m,i-1/2,j,k}^y) + \frac{3\eta_m}{\Delta y_j} (\psi_{m,i,j+1/2,k}^y + \psi_{m,i,j-1/2,k}^y - 2\psi_{m,i,j,k}^y) \\ + \frac{\xi_m}{\Delta z_k} (\psi_{m,i,j,k+1/2}^y - \psi_{m,i,j,k-1/2}^y) + \sigma_{t,i,j,k} \psi_{m,i,j,k}^y = S_{m,i,j,k}^y \end{aligned} \quad (4)$$

$$\begin{aligned} \frac{\mu_m}{\Delta x_i} (\psi_{m,i+1/2,j,k}^z - \psi_{m,i-1/2,j,k}^z) + \frac{\eta_m}{\Delta y_j} (\psi_{m,i,j+1/2,k}^z - \psi_{m,i,j-1/2,k}^z) \\ + \frac{3\xi_m}{\Delta z_k} (\psi_{m,i,j,k+1/2}^z + \psi_{m,i,j,k-1/2}^z - 2\psi_{m,i,j,k}^z) + \sigma_{t,i,j,k} \psi_{m,i,j,k}^z = S_{m,i,j,k}^z \end{aligned} \quad (5)$$

where,

$$\psi_{m,i,j,k} \equiv \frac{1}{\Delta x_i \Delta y_j \Delta z_k} \int_{x_{i+1/2}}^{x_{i+3/2}} \int_{y_{j-1/2}}^{y_{j+1/2}} \int_{z_{k-1/2}}^{z_{k+1/2}} \psi_m(x, y, z) dx dy dz, \quad (6)$$

and

$$\psi_{m,i,j,k}^n \equiv \frac{3}{\Delta x_i \Delta y_j \Delta z_k} \int_{x_{i+1/2}}^{x_{i+3/2}} \int_{y_{j-1/2}}^{y_{j+1/2}} \int_{z_{k-1/2}}^{z_{k+1/2}} P_i(n) \psi_m(x, y, z) dz dy dx, \quad n = x, y, z. \quad (7a-7c)$$

The definitions for the source moments are obtained by replacing ψ with S in Eqs. (6)-(7). The average and first spatial angular fluxes moments on the outgoing faces are defined as:

$$\Psi_{m,i+1/2,j,k} \equiv \frac{1}{\Delta y_j \Delta z_k} \int_{y_{j-1/2}}^{y_{j+1/2}} \int_{z_{k-1/2}}^{z_{k+1/2}} \psi_m(x_{i+1/2}, y, z) dz dy, \quad (8)$$

$$\Psi_{m,i+1/2,j,k}^n \equiv \frac{1}{\Delta y_j \Delta z_k} \int_{y_{j-1/2}}^{y_{j+1/2}} \int_{z_{k-1/2}}^{z_{k+1/2}} P_i(n) \psi_m(x_{i+1/2}, y, z) dz dy, \quad n = y, z, \quad (9a-9b)$$

$$\Psi_{m,i,j+1/2,k} \equiv \frac{1}{\Delta x_i \Delta z_k} \int_{x_{i-1/2}}^{x_{i+1/2}} \int_{z_{k-1/2}}^{z_{k+1/2}} \psi_m(x, y_{j+1/2}, z) dz dx, \quad (10)$$

$$\Psi_{m,i,j+1/2,k}^n \equiv \frac{1}{\Delta x_i \Delta z_k} \int_{x_{i-1/2}}^{x_{i+1/2}} \int_{z_{k-1/2}}^{z_{k+1/2}} P_i(n) \psi_m(x, y_{j+1/2}, z) dz dx, \quad n = x, z, \quad (11a-11b)$$

$$\Psi_{m,j,k+1/2} \equiv \frac{1}{\Delta y_j \Delta x_i} \int_{y_{j-1/2}}^{y_{j+1/2}} \int_{x_{i-1/2}}^{x_{i+1/2}} \psi_m(x, y, z_{k+1/2}) dx dy, \quad (12)$$

$$\Psi_{m,i,j,k+1/2}^n \equiv \frac{1}{\Delta y_j \Delta x_i} \int_{y_{j-1/2}}^{y_{j+1/2}} \int_{x_{i-1/2}}^{x_{i+1/2}} P_i(n) \psi_m(x, y, z_{k+1/2}) dx dy, \quad n = y, x. \quad (13a-13b)$$

At this point, we have four equations with thirteen unknowns. To obtain the auxiliary equations we assume an exponential representation for the angular flux within each cell. Using information theory⁶, we find that this representation is given by

$$\psi_m(x, y, z) = a_{m,i,j,k} e^{\lambda_{m,i,j,k}^x P_i(x) + \lambda_{m,i,j,k}^y P_j(y) + \lambda_{m,i,j,k}^z P_j(z)}. \quad (14)$$

To find $a_{m,i,j,k}$, $\lambda_{m,i,j,k}^x$, $\lambda_{m,i,j,k}^y$ and $\lambda_{m,i,j,k}^z$, we apply our definitions for the zeroth, x, y and z spatial moments of the angular flux. Inserting Eq.(14) into Eqs.(6) - (7), we obtain

$$a_{m,i,j,k} = \psi_{m,i,j,k} \frac{\lambda_{m,i,j,k}^x}{\sinh(\lambda_{m,i,j,k}^x)} \frac{\lambda_{m,i,j,k}^y}{\sinh(\lambda_{m,i,j,k}^y)} \frac{\lambda_{m,i,j,k}^z}{\sinh(\lambda_{m,i,j,k}^z)}, \quad (15)$$

and

$$\frac{\psi_{m,i,j,k}^n}{\psi_{m,i,j,k}} = 3 \left[\coth(\lambda_{m,i,j,k}^n) - \frac{1}{\lambda_{m,i,j,k}^n} \right], \quad n = x, y, z. \quad (16a-16c)$$

Next, we use Eq.(14) to obtain our auxiliary equations. We assume that the angular fluxes are discontinuous at the edges of the cell. Inserting Eq.(14) into Eqs.(8) to (13) gives the following nine auxiliary equations:

$$\psi_{m,i\pm 1/2,j,k} = \psi_{m,i,j,k} \frac{\lambda_{m,i,j,k}^x}{\sinh(\lambda_{m,i,j,k}^x)} e^{\pm \lambda_{m,i,j,k}^x}, \quad \mu_m > 0, \quad (18)$$

$$\psi_{m,i\pm 1/2,j,k}^n = \psi_{m,i,j,k}^n 3 \left[\coth(\lambda_{m,i,j,k}^n) - \frac{1}{\lambda_{m,i,j,k}^n} \right] \frac{\lambda_{m,i,j,k}^x}{\sinh(\lambda_{m,i,j,k}^x)} e^{\pm \lambda_{m,i,j,k}^x}, \quad n = y, z, \quad \mu_m > 0, \quad (19a-19b)$$

$$\psi_{m,i,j\pm 1/2,k} = \psi_{m,i,j,k} \frac{\lambda_{m,i,j,k}^y}{\sinh(\lambda_{m,i,j,k}^y)} e^{\pm \lambda_{m,i,j,k}^y}, \quad \eta_m > 0, \quad (20)$$

$$\psi_{m,i\pm 1/2,j,k}^n = \psi_{m,i,j,k}^n 3 \left[\coth(\lambda_{m,i,j,k}^n) - \frac{1}{\lambda_{m,i,j,k}^n} \right] \frac{\lambda_{m,i,j,k}^y}{\sinh(\lambda_{m,i,j,k}^y)} e^{\pm \lambda_{m,i,j,k}^y}, \quad n = x, z, \quad \eta_m > 0, \quad (21a-21b)$$

$$\psi_{m,i,j,k\pm 1/2} = \psi_{m,i,j,k} \frac{\lambda_{m,i,j,k}^z}{\sinh(\lambda_{m,i,j,k}^z)} e^{\pm \lambda_{m,i,j,k}^z}, \quad \xi_m > 0, \quad (22)$$

$$\psi_{m,i,j,k\pm 1/2}^n = \psi_{m,i,j,k}^n 3 \left[\coth(\lambda_{m,i,j,k}^n) - \frac{1}{\lambda_{m,i,j,k}^n} \right] \frac{\lambda_{m,i,j,k}^z}{\sinh(\lambda_{m,i,j,k}^z)} e^{\pm \lambda_{m,i,j,k}^z}, \quad n = x, y, \quad \xi_m > 0. \quad (23a-23b)$$

To summarize, the ED equations are given by Eq.(2)-(5),(16) and (18)-(23).

The ED equations are solved somewhat differently than existing linear differencing schemes since it is inherently nonlinear. As with most discrete-ordinates schemes, we use source-iteration (SI) to iteratively solve for the scattering source. However, for within cell calculations, the ED equations are solved using Newton-Raphson iterations for the cell average scalar fluxes and moments and the scalar fluxes and

moments on the outgoing faces. All within cell Newton-Raphson iterations are initialized with $\lambda_x, \lambda_y, \lambda_z = 0$, which from practical experience appears to be the most robust. Current studies are ongoing to obtain a diffusion accelerated solution method for the ED scheme. This has been done in slab geometry but has not been extended to multidimensional geometries.

Having coded the ED scheme and solution method, we encountered difficulties with problems with anisotropic scattering, when the truncated Legendre expansion of the discrete-ordinate source leads to negative sources. In order for a solution to be possible, the ED scheme requires that the solution be positive everywhere or negative everywhere. This results from information theory (maximum entropy). Therefore, it appears that solutions to the ED scheme can only be obtained if the scattering source is positive everywhere in the problem. Current investigations are ongoing to obtain positive discrete-ordinate sources regardless of the Legendre expansion of the scattering source.

III. Numerical Results

In this section we provide results for one test problem. We compare the ED scheme with the linear discontinuous (LD), constant-linear nodal with negative flux fix-up (CLN/F) and adaptive weighted diamond difference (AWDD) schemes. The LD scheme does not use any negative flux fixup method. We cannot compare with the NC/EC scheme since it has not been developed and implemented in x-y-z geometry with hexahedral meshes.

The physical problem is a 120-cm cube of an iron alloy, in which is centered a 119-cm cube of an aqueous solution, in which is centered a 40-cm cube of the iron alloy, in which is centered a 10-cm cube of the aqueous solution that contains the source. Symmetry allows us to consider only one octant (a 60-cm cube) with reflecting boundaries on the bottom, left and front sides and vacuum boundaries on the top, right and back sides. The source emits 73.9 % of its neutrons in the first of three energy groups, with the remaining 26.1 % in the second energy group. We use an S4 quadrature set and isotropic scattering cross sections. The cross sections for the aqueous solution are given in Table 1 and the cross section for the iron alloy are given in Table 2. All calculations are converged to a relative error of 10^{-3} .

In Figures 1 to 3 we present some results for the this test problem. Here, for each energy group, the scalar flux is given, for various mesh sizes, at a detector located at $59.5 \text{ cm} \leq x \leq 60.0 \text{ cm}$, $59.5 \text{ cm} \leq y \leq 60.0 \text{ cm}$, and $59.5 \text{ cm} \leq z \leq 60.0 \text{ cm}$. The coarsest mesh is $5 \times 5 \times 5$ (5 cells along each spatial axis) and the finest mesh is $57 \times 57 \times 57$. If a data point representing the solution for a given scheme at a given mesh does not appear on the graph, then it lies outside the domain of the graph or was a negative value. Negative solutions only appeared for the LD scheme. We observe that the ED scheme is far more accurate than the other schemes especially at the coarse meshes. Obtaining accurate fluxes at such localized locations is much more difficult than an integral quantity, such as the total leakage, especially in a deep-penetration problem such as this. We note that the ED scheme did not generate any negative fluxes. We also note that the error in the ED solution was never more than a factor of two for the coarsest meshes; all other scheme were off by several orders of magnitude at the coarsest meshes. Also, the AWDD scheme is not monotonically converging at the refined meshes.

For this problem the ED scheme took, on average, 4 times longer than the CLN/F scheme and 10 times longer than the AWDD on a per cell, per angle basis. Timing comparisons were not made with the LD scheme, since the implementation is not optimized for accurate comparisons.

IV. DISCUSSION

We have extended the ED scheme to x-y-z geometry with hexahedral meshes and implemented it into the THREEDANT™ code. One of the main advantages of the ED scheme is that it produces strictly positive angular fluxes. We have tested the scheme on a variety of problems, including the one in this paper, and have found that it is very accurate for deep-penetration problems with optically thick spatial meshes.

We are in the process of extending the ED scheme to x-y-z geometry with unstructured tetrahedral meshes.

ACKNOWLEDGMENTS

This work was performed under the auspices of the U.S. Department of Energy.

REFERENCES

- 1.) W. F. Walters, and T. A. Wareing, "A Nonlinear Positive Method for Solving the Transport Equation on Coarse Meshes," Proceedings Eighth International Conference on Radiation Shielding, Vol 1, Arlington, Texas (1994).
- 2.) W. F. Walters and T. A. Wareing, "An Accurate, Strictly-Positive, Nonlinear Characteristic Scheme for the Discrete-Ordinates Equations," *Transport Theory and Statistical Physics*, accepted for publication (1994).
- 3) W.F. Walters, T.A. Wareing and D.R. Marr, "The Nonlinear Characteristic Scheme for X-Y Geometry Transport Problems", Proceedings International Conference on Mathematics and Computations, Reactor Physics and Environmental Analyses, Portland, Oregon, April 30-May 4, (1995).
- 4) B.M. Minor, "Exponential Characteristic Spatial Quadrature for Discrete Ordinates Neutral Particle Transport in Two-Dimensional Cartesian Coordinates", Ph.D. Dissertation, Air Force Institute of Technology, AFIT/DS/ENP/93-7, (1993).
- 5) K.A. Mathews, G.A. Sjoden, and B.M. Minor, "Exponential Characteristic Spatial Quadrature for Discrete Ordinates Radiation Transport in Slab Geometry", *Nucl. Sci. Eng.*, **118**, 24-37, (1994).
- 6.) E.T. Jaynes, "Information Theory and Statistical Mechanics", *Phys. Rev.*, **106**, 620, (1957).
- 7.) T.A. Wareing and W.F. Walters, "An Exponential Discontinuous Scheme for X-Y Geometry Transport Problems", *Trans. Am. Nucl. Soc.*, Philadelphia, Pennsylvania, Vol 72, (1995).
- 8.) R.E. Alcouffe, et al, "DANTSYS: A Diffusion Accelerated Neutral Particle Transport Code System", LA-12969-M, Los Alamos National Laboratory, (1995).

Table 1: Cross Section Data for Aqueous Solution

Group Number (g)	$\sigma_{t,g}$	$\sigma_{s,g \rightarrow g}$	$\sigma_{s,(g-1) \rightarrow g}$
1	0.2656	0.1600	0.0000
2	1.1745	0.8220	0.1052
3	3.2759	2.2980	0.0730

Table 2: Cross Section Data for Iron Alloy

Group Number (g)	$\sigma_{t,g}$	$\sigma_{s,g \rightarrow g}$	$\sigma_{s,(g-1) \rightarrow g}$
1	0.2163	0.1760	0.0000
2	0.3255	0.2500	0.0399
3	1.1228	0.7982	0.0001

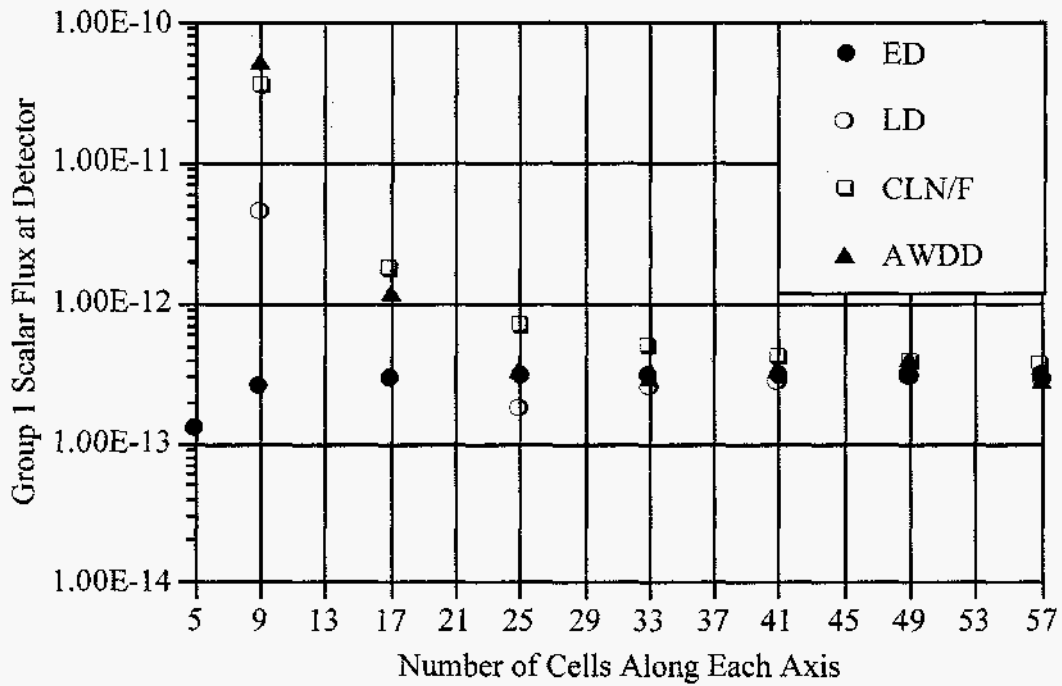


Figure 1: Group 1 Scalar Fluxes at the Detector Location

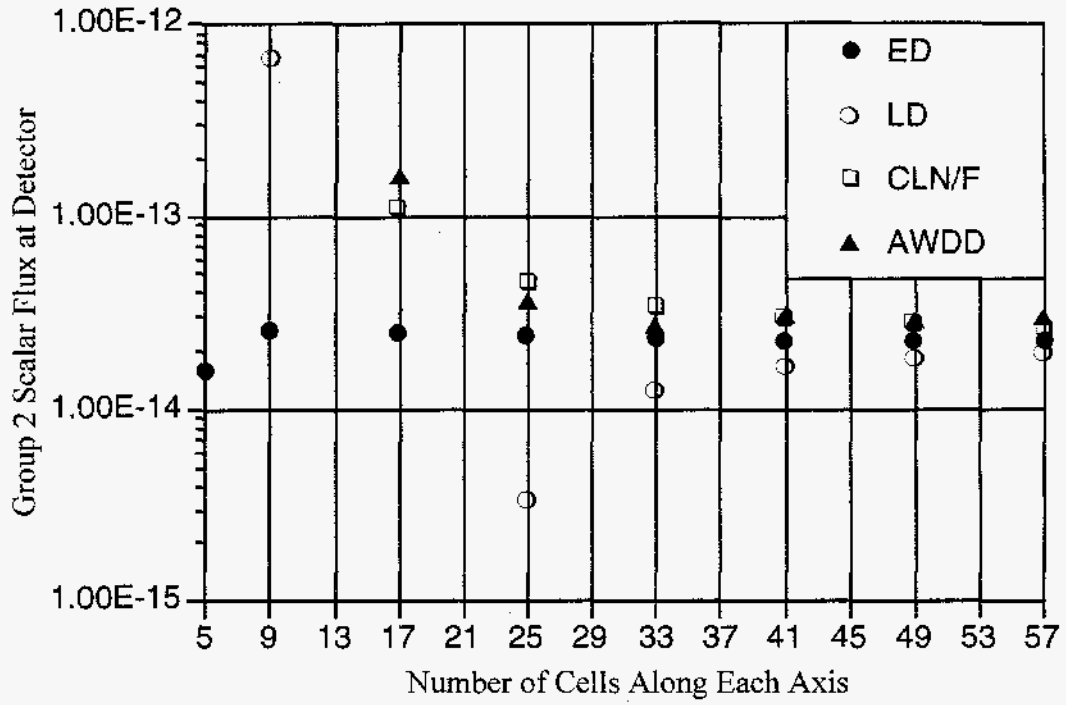


Figure 2: Group 2 Scalar Fluxes at the Detector Location

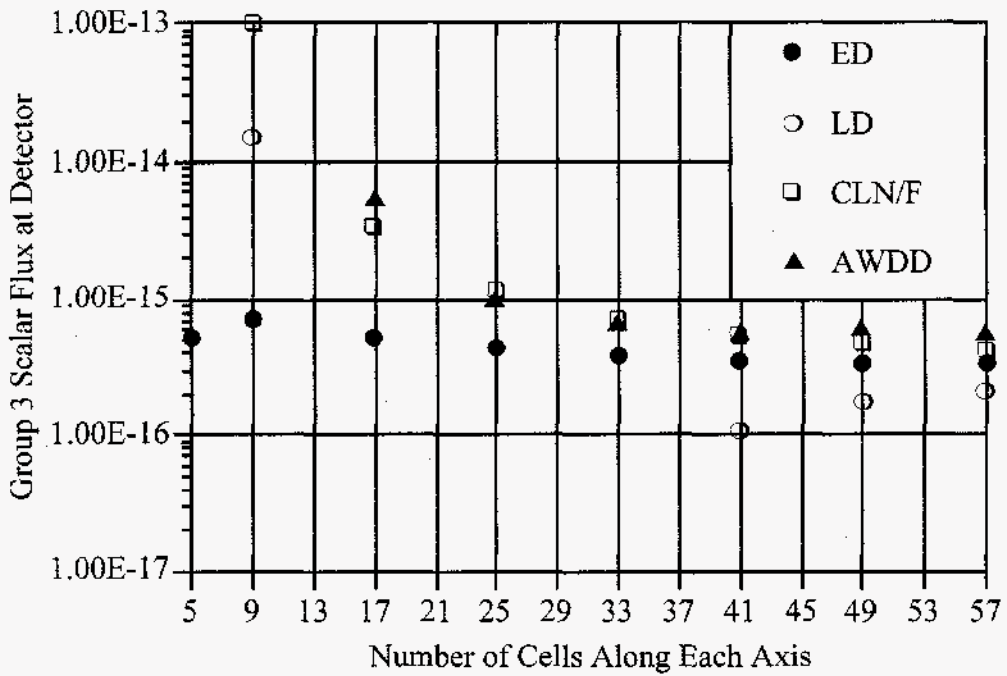


Figure 3: Group 3 Scalar Fluxes at the Detector Location